Acta Crystallographica Section B
Structural Science
ISSN 0108-7681

Experimental electron density in the triclinic phase of $Co_2(CO)_6(\mu\text{-}CO)(\mu\text{-}C_4O_2H_2)$ at 120 K

Riccardo Bianchi,[a] Giuliana Gervasio[b] and Domenica Marabello[b]*

[a]Centro CNR per lo Studio delle Relazioni tra Struttura e Reattività Chimica, via Golgi 19, I-20133 Milano, Italy, and [b]Dipartimento di Chimica IFM dell'Università, via P. Giuria 7, I-10125 Torino, Italy

Correspondence e-mail: marabello@ch.unito.it

Received 8 January 2001
Accepted 1 June 2001

The experimental electron density (ED) of the triclinic phase of $Co_2(CO)_6(\mu\text{-}CO)(\mu\text{-}C_4O_2H_2)$, μ-carbonyl-μ-5-oxo-2,5-dihydrofuran-2-ylbis(tricarbonylcobalt), has been determined through X-ray diffraction at 120 K. The presence of a 'closed shell' Co—Co bond in the title compound, found in an experimental ED study of its orthorhombic form, is confirmed by the Quantum Theory of Atoms in Molecules. However, the two phases show a significant Co—Co bond length difference [triclinic: 2.4402 (2) Å; orthorhombic: 2.4222 (3) Å]. The flat distribution of the experimental ED along the Co—Co bond path and on the two Co_2C rings allows for variations of the Co—Co bond length which may be easily induced by the different packing arrangements of the two forms.

1. Introduction

In the reaction of $Co_2(\mu\text{-}CO)_2(CO)_6$ (1) (Gardner Sumner *et al.*, 1964; Braterman, 1972) with acetylene the well known compound $Co_2(CO)_6(\mu\text{-}\eta^2\text{-}HC{\equiv}CH)$ (2) (Greenfield *et al.*, 1956) is obtained, where the C≡C bond is perpendicular to the metal–metal bond. A subsequent reaction of (2) with CO yields the product $Co_2(CO)_6(\mu\text{-}CO)(\mu\text{-}C_4O_2H_2)$ (3) (Sternberg *et al.*, 1959), which is an intermediate in the catalytic cycle to produce bisfurandiones (Pályi *et al.*, 1986). From the reaction mixture two polymorphic forms of complex (3) were obtained: one was orthorhombic and the other was triclinic. The crystal structure of the triclinic phase was determined by Mills & Robinson (1967). The Effective Atomic Number (EAN) rule suggests the presence of a Co—Co bond in the dinuclear complexes (1), (2) and (3) which have different bridging groups.

Until now, theoretical (Heijser *et al.*, 1980; Low *et al.*, 1991) and experimental (Leung & Coppens, 1983) calculations on dicobalt complexes with bridging ligands gave no evidence for the presence of a Co—Co bond. *Ab initio* calculations on $(\eta^5\text{-}C_5H_5)_2Co_2(\mu\text{-}NO)_2$ (Low & Hall, 1993) and on $Co_2(CO)_8$ (Low *et al.*, 1991) showed that at certain geometries and levels of electron correlation a Co—Co bond exists, but at other geometries and levels of electron correlation the Co—Co bond vanishes. This behavior evidences the flat nature of the electron density inside the $Co_2(\mu\text{-}X)_2$ (X = C, N) ring.

Recently, in order to give an answer to the presence of an M—M bond in unsupported and supported dinuclear transition metal complexes, we determined the experimental elec-

Table 1
Experimental details.

Crystal data	
Chemical formula	$C_{11}H_2Co_2O_9$
Chemical formula weight	395.99
Cell setting, space group	Triclinic, $P\overline{1}$
a, b, c (Å)	7.169 (2), 8.452 (2), 11.364 (3)
α, β, γ (°)	82.77 (1), 80.84 (1), 87.72 (2)
V (Å^3)	674.3 (3)
Z	2
D_x (Mg m^{-3})	1.942
Radiation type	Mo $K\alpha$
No. of reflections for cell parameters	35
θ range (°)	10–15
μ (mm^{-1})	2.493
Temperature (K)	120 (2)
Crystal form, color	Prismatic, red
Crystal size (mm)	0.40 × 0.36 × 0.24
Data collection	
Diffractometer	Siemens P4
Data collection method	$\theta/2\theta$ scans
Absorption correction	Numerical
T_{min}	0.373
T_{max}	0.601
No. of measured, independent and observed parameters	35 370, 11 623, 5479
Criterion for observed reflections	$I > 3\sigma(I)$
R_{int}	0.034
θ_{max} (°)	48.5
Range of h, k, l	$-15 \rightarrow h \rightarrow 10$ $-19 \rightarrow k \rightarrow 19$ $-26 \rightarrow l \rightarrow 21$
No. and frequency of standard reflections	7 every 50 reflections
Intensity decay (%)	0
Refinement	
Refinement on	F^2
$R[F^2>3\sigma(F^2)]$, $wR(F^2)$, S	0.0239, 0.0301, 0.867
No. of reflections and parameters used in refinement	5479, 571
H-atom treatment	Mixed
Weighting scheme	$1/\sigma^2$
$(\Delta/\sigma)_{max}$	0.01
$\Delta\rho_{max}$, $\Delta\rho_{min}$ (e Å^{-3})	0.4, −0.1

tron density (ED) of $Mn_2(CO)_{10}$ (Bianchi *et al.*, 1998, 2000) and of the orthorhombic phase of (3) (Bianchi *et al.*, 2001); the subsequent topological analyses of the experimental ED showed for the first time the presence of an $M-M$ bond (Bianchi *et al.*, 1998, 2000, 2001). For unsupported dinuclear transition metal complexes this result was confirmed by other experimental works (Macchi *et al.*, 1998, 1999).

Here, we report on the experimental ED study of the triclinic form of (3) to confirm the results earlier obtained for its orthorhombic phase and to see if new insight can be obtained on the bonding differences between the two mentioned phases.

2. Experimental

2.1. Data collection

Complex (3) (triclinic and orthorhombic forms) crystallizes at 263 K from a solution of hexane. A red crystal (0.24 × 0.36 × 0.40 mm) of the triclinic form was placed in a Lindemann glass capillary and the intensity data were collected with graphite-monochromated Mo $K\alpha$ radiation (λ = 0.71073 Å), using the θ–2θ scan method on a Siemens P4 diffractometer equipped with a N_2 gas-stream low-temperature device. The crystal data are collected in Table 1.

The crystal was cooled to 120 K over ∼4 h; 35 370 reflections were collected up to $\sin\theta/\lambda$ = 1.054 Å^{-1} (limiting indices $-15 < h < 15$, $-17 < k < 17$, $-23 < l < 23$), scan width = 2.2° and variable scan speed (2.00–15.00° min^{-1}). Seven standard reflections were measured every 50 reflections and no crystal decay occurred. A local program was used as the interface between the output data of profiles yielded by the *XSCANS* data collection program (Siemens, 1996) and the package of programs (*REFPK*, *BGLP*, *TSCALE*, *SORTAV*) used for data reduction (Blessing, 1987, 1989). The absorption correction was made by numerical integration using the *ABSORB* program (De Titta, 1985). The independent reflections were 11 623 ($R_{int} = \Sigma_{hkl}||F_o|^2 - |F_o|^2_{(mean)}|/\Sigma_{hkl}|F_o|^2 = 0.034$).

2.2. Refinements

All refinements were carried out using the *VALRAY* program implemented by Stewart & Spackman (1983). The minimized quantity was $\Sigma w(|F_o|^2 - k^2|F_c|^2)^2$ based on 4921 reflections with $I > 3\sigma(I)$ and weights $w = 1/\sigma^2(|F_o|^2)$. Extinction was found to be negligible.

The structure of complex (3) was refined first by a full-matrix least-squares method using the spherical independent atom model (IAM). The atomic scattering factors and anomalous dispersion coefficients were taken from *International Tables for X-ray Crystallography* (1974). Agreement factors and other informations on data refinements are given in Table 2. An *ORTEP* plot of the molecular structure of (3) is shown in Fig. 1.

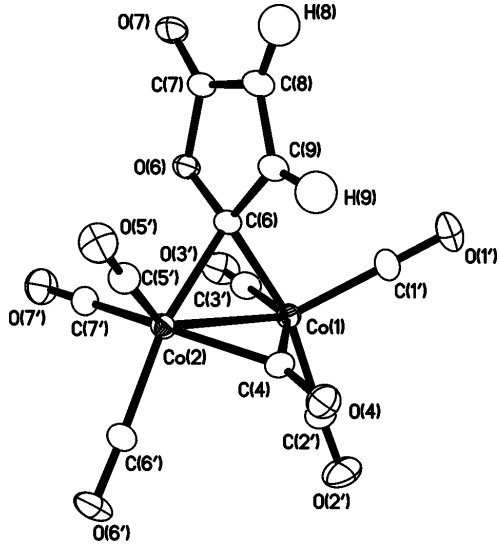

Figure 1
An *ORTEP* (Johnson, 1965) plot of $Co_2(CO)_6(\mu\text{-}CO)(\mu\text{-}C_4O_2H_2)$ (3).

Table 2
IAM and multipole refinement information.

N_o (No. of reflections)	4921	
Refinement model	IAM	Multipole
N_p (No. of parameters)	207	579
$R(F) = \Sigma \|\|F_o\| - k\|F_c\|\|/\Sigma\|F_o\|$	0.0322	0.0239
$wR(F) = [\Sigma w(\|F_o\| - k\|F_c\|)^2/\Sigma w\|F_o\|^2]^{1/2}$	0.0415	0.0301
$R(F^2) = \Sigma\|\|F_o\|^2 - k^2\|F_c\|^2\|/\Sigma\|F_o\|^2$	0.0495	0.0303
$wR(F^2) = [\Sigma w(\|F_o\|^2 - k^2\|F_c\|^2)^2/\Sigma w\|F_o\|^4]^{1/2}$	0.0794	0.0591
$S = [\Sigma w(\|F_o\|^2 - k^2\|F_c\|^2)^2/(N_o - N_p)]^{1/2}$	1.119	0.867
k (scale factor)	0.896 (1)	0.906 (2)
$(\text{shift/e.s.d.})_{\max}$	< 0.01	< 0.01

The final aspherical fit to the triclinic X-ray data of (3) was obtained with the following multipole model. Multipoles were included up to the hexadecapole level for the Co atoms, whereas the expansions were limited to octupoles for C and O atoms and to dipoles for H atoms. To each Co, O and C atom were assigned two monopoles (one termed 'core' and the other 'valence'). The monopole scattering factors were calculated using fixed linear combinations of Slater-type radial density functions derived from the Hartree–Fock atomic wavefunctions of Clementi & Roetti (1974). A single core population parameter was refined for the core of all C and O atoms, while the core population parameter of each Co atom was constrained to twice the corresponding valence population parameter. For the higher multipoles, the radial scattering factors of all atoms were obtained from single Slater-type density functions. The Slater-type α exponents, of Co, O, C and H atoms, were assigned fixed values based on theory (Hehre *et al.*, 1970). Each H monopole was a single shell, given by $\exp(-2.48r)$. A number of other models were tested before deciding on this model. For example we tried:

(i) to refine the Slater-type α exponent of Co atoms;

(ii) to optimize a radial scale factor for each valence function of C and O atoms, as in the k refinement model (Hansen & Coppens, 1978), subject to the constraint of the equal scale factor (but different populations) for all atoms of the same type;

(iii) to impose constraints to the higher multipole parameters of the atoms located in an approximate m site symmetry environment (the atoms of the γ-lactonic ring and of the bridging CO).

However, such refinements did not improve the residuals nor did they lead to significant differences in the topological features discussed below.

The scale factor k was estimated by the sum of the monopole populations divided by $F(000)$. The positional and the anisotropic thermal parameters of Co, O and C atoms were varied. H-atoms positions were fixed to those obtained by a previous refinement where the H atoms are polarized in the direction of the atom to which they are bonded, and only their isotropic thermal parameters were refined. Introduction of anharmonic parameters leads only to a marginal drop in the R factor and no significant improvement in the multipole analysis, so they were excluded from the final model. Information on the multipole refinement is given in Table 2. A list of all refined parameters and maps based on $F_{\text{observed}} - F_{\text{IAM}}$, $F_{\text{multipole}} - F_{\text{IAM}}$ and $F_{\text{observed}} - F_{\text{multipole}}$ (not reported in this paper) are given as supplementary materials.[1] The atomic fractional coordinates and the thermal parameters from the multipolar refinement are also given as supplementary materials. Hirshfeld's rigid-bond test (Hirshfeld, 1976) applied in an analysis of the atomic displacement parameters was positive. The r.m.s. of differences $\Delta z^2_{A,B}$'s for all bonded pairs is 0.0014 Å^2; where $\Delta z^2_{A,B} = z^2_{A,B} - z^2_{B,A}$, *i.e.* the difference between the mean square vibration amplitudes along the mutual bond of the A and B atoms (see supplementary material).

2.3. Topological analysis

The experimental ED, $\rho(\mathbf{r})$, and its gradient and Hessian were calculated with a direct space lattice sum from the multipole parameters. The Quantum Theory of Atoms in Molecules (QTAM; Bader, 1990) allows quantitative structural information from the experimental ED and it can be used for the analysis of the atomic interactions in the crystals. Of particular importance for the analysis are the critical points where the gradient of the density vanishes, $\nabla\rho(\mathbf{r}) = 0$. They can be denoted by a couple of integers (r,s): the rank (r) is the number of non-zero eigenvalues of the Hessian matrix and the signature (s) is the sum of the signs of the eigenvalues. A (3,+1) critical point is the point where $\rho(\mathbf{r})$ attains its minimum value on a ring surface and is thus termed *ring critical point*. The definition of the chemical bond is based on the existence of a (3,−1) critical point (BCP) along a line of maximum density (bond path) linking the nuclei of neighboring atoms. At the BCP the sum of the three eigenvalues (two negative, λ_1 and λ_2, and one positive, λ_3) of the density Hessian matrix yields the Laplacian value, $\nabla^2\rho_b$ [$\rho_b = \rho(\mathbf{r})$ at the BCP]. The eigenvalues λ_i measure the contraction of the $\rho(\mathbf{r})$ towards the BCP in a plane perpendicular to the bond path (λ_1 and λ_2) or along it (λ_3).

The topology of $\nabla^2\rho(\mathbf{r})$ allows the characterization of local concentrations [$\nabla^2\rho(\mathbf{r}) < 0$] and depletions [$\nabla^2\rho(\mathbf{r}) > 0$] of the $\rho(\mathbf{r})$. In 'shared' interactions, where ρ_b is high and $\nabla^2\rho_b < 0$, there is a lowering of the potential energy density, $V(\mathbf{r})$, associated with a concentration in charge between the nuclei along the bond path. 'Closed-shell' interactions, where ρ_b is low and $\nabla^2\rho_b > 0$, are dominated by the kinetic energy in the region of the interatomic surface. Additional information on chemical bonds is available from the kinetic energy density G_b, the potential energy density V_b and the total energy density $E^e_b = G_b + V_b$, calculated at the BCP position. They cannot be rigorously derived from a knowledge of just the density and they were thus obtained using an empirical functional theory from Abramov (1997) and Espinosa (Espinosa *et al.*, 1998). The covalent bonds show relatively large values of ρ_b and large negative values of $\nabla^2\rho_b$. These 'shared' interactions have

[1] Supplementary data for this paper are available from the IUCr electronic archives (Reference: LC0036). This includes multipolar population parameters, the differences of the projections of the thermal displacements for bonded atoms, residual and deformation maps and figures of the crystal packing (not reported in the text). Services for accessing these data are described at the back of the journal.

negative E_b^e, being dominated by large negative V_b associated with charge concentration in the internuclear region. Instead the ionic bonds have relatively low ρ_b and positive $\nabla^2\rho_b$, as the density contracts away from the contact region of the interacting atoms. These 'closed-shell' interactions are dominated by the kinetic energy in the region of the BCP with G_b slightly greater than $|V_b|$ and with E_b^e positive and close to zero. The electron density topological properties were derived using the program *PAMoC* (Barzaghi, 2001).

3. Results and discussion

3.1. Structural properties

In (3) the two $Co(CO)_3$ moieties (Fig. 1) are bridged by a carbonyl group and by a γ-lactonic ring, almost planar (the mean deviation from planarity is 0.0078 Å) and nearly perpendicular (88°) to the Co–Co line. A molecule of (3) has an approximate symmetry plane containing the γ-lactonic ring and the bridging CO group; a double bond is localized between C(8) and C(9) atoms. The two Co_2C rings make an angle of 111°.

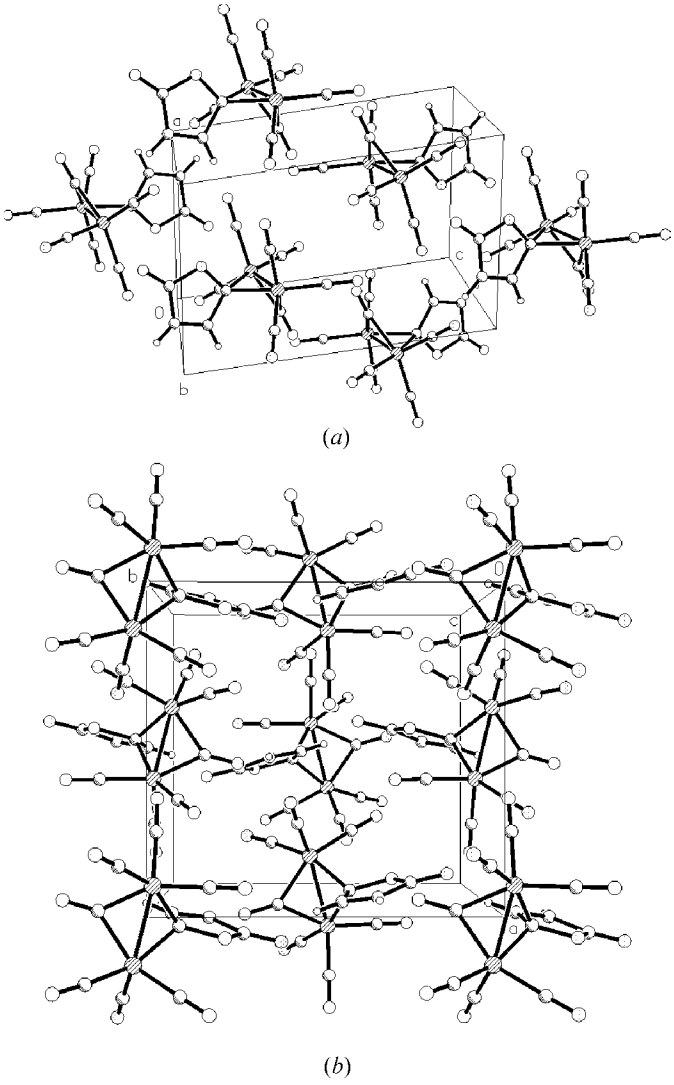

Figure 2
Crystal packing of (*a*) triclinic and (*b*) orthorhombic forms of $Co_2(CO)_6(\mu\text{-}CO)(\mu\text{-}C_4O_2H_2)$ (3).

Table 3
Intermolecular $X\cdots Y$ contacts from the multipole refinement.

Contacts marked with an asterisk correspond to interactions whose bond paths and BCP's were found from the topological analysis of $\rho(\mathbf{r})$.

O(6)···O(7)^{i}	3.127 (3)	O(4)···O(3′)^{v}	3.192 (5)*
O(6)···O(5′)^{ii}	3.316 (4)	O(4)···O(7′)^{v}	3.240 (5)*
C(7)···C(7)^{i}	3.264 (3)	O(4)···C(6′)^{vi}	3.214 (4)
C(7)···O(7)^{i}	3.190 (4)	O(4)···O(6′)^{vi}	3.024 (4)*
O(7)···C(1′)^{i}	3.056 (4)	C(1′)···O(3′)^{v}	3.412 (5)
O(7)···O(1′)^{i}	3.188 (5)	C(1′)···O(6′)^{vii}	3.316 (4)
O(7)···C(3′)^{i}	3.034 (3)	O(1′)···O(2′)^{viii}	3.058 (5)
O(7)···O(3′)^{i}	3.179 (5)	O(1′)···O(3′)^{v}	3.133 (6)*
O(7)···C(5′)^{ii}	3.088 (4)*	O(1′)···C(5′)^{vii}	3.341 (3)
O(7)···O(5′)^{ii}	3.154 (4)	O(1′)···O(5′)^{vii}	3.250 (4)*
C(8)···O(5′)^{iii}	3.193 (4)*	O(1′)···C(6′)^{vii}	3.321 (4)
C(8)···O(7′)^{ii}	3.344 (4)*	O(1′)···O(6′)^{vii}	3.164 (5)*
H(8)···O(1′)^{iv}	2.71 (4)*	O(2′)···C(7′)^{ix}	3.289 (4)
H(8)···O(3′)^{i}	2.89 (4)	O(2′)···O(7′)^{ix}	3.108 (5)*
H(8)···O(5′)^{iii}	2.87 (3)	O(2′)···C(6′)^{ix}	3.359 (5)
C(9)···O(5′)^{iii}	3.190 (4)	O(2′)···O(6′)^{ix}	3.201 (6)*
H(9)···O(3′)^{v}	2.83 (4)*	C(5′)···O(7′)^{v}	3.356 (5)
H(9)···O(5′)^{iii}	2.86 (3)	O(5′)···O(5′)^{iii}	3.294 (4)*
C(4)···O(4)^{vi}	3.309 (3)	O(5′)···O(7′)^{v}	3.084 (5)*
O(4)···O(4)^{vi}	3.078 (4)*	O(5′)···O(7′)^{ii}	3.046 (4)*
O(4)···C(2′)^{vi}	3.277 (3)	O(3′)···O(6′)^{ix}	3.331 (5)*
O(4)···O(2′)^{vi}	3.096 (5)*		

Symmetry codes: (i) $1-x, 2-y, -z$; (ii) $1-x, 1-y, -z$; (iii) $-x, 1-y, -z$; (iv) $-x, 2-y, -z$; (v) $-1+x, y, z$; (vi) $-x, 1-y, 1-z$; (vii) $x, 1+y, z$; (viii) $-x, 2-y, 1-z$; (ix) $1-x, 1-y, 1-z$.

Bond distances and angles obtained from the multipole refinement have been deposited and the intermolecular contacts (< 3.4 Å) are listed in Table 3. The crystal packing shows very weak intermolecular C—H···O interactions and a prevalence of the O···O contacts. The C—H···O interactions have large values of the H···O distances with C···O distances ranging from 3.19 to 3.78 Å, typical values for these types of interactions (Desiraju, 1991).

The orthorhombic (Bianchi *et al.*, 2001) and the triclinic form differ significantly in the cobalt–cobalt distance [2.4222 (3) and 2.4402 (2) Å, respectively] and in the crystal packing interactions as discussed below. The two crystal packings are shown in Fig. 2.

3.2. Atomic charges

The electron population of individual atoms was calculated, but it is model dependent and has limited physical significance. However, when the electron density is partitioned into atomic group components, the resulting estimates of group charges should be correspondingly less model dependent.

Net atomic charges, defined as the atomic number Z minus the atomic electron population, are given in Table 4. The Co atoms and the carbonyl ligands can be individually considered neutral within experimental error (3σ). However, significant and slightly positive [0.60 (14) e] and negative [−0.83 (21) e] charges are globally concentrated on the two cobalts and on the γ-lactonic ring, respectively.

3.3. Deformation densities

The average $\sigma(\Delta\rho(\mathbf{r}))$ (Cruickshank, 1949) for bonding regions is 0.08 e Å^{-3}. The largest peak [close to the Co(1) atom] in the residual map (based on $F_{obs} - F_{mult}$) is 0.26 e Å^{-3} and it is slightly greater than 3σ. However, no other significant features are present in the residual map (see, for example, Fig. 3). The model deformation density maps (based on $F_{mult} - F_{IAM}$) in the Co(1)Co(2)C(4) and in the γ-lactonic planes (Fig. 4) show the electron accumulation due to bonding between the atoms.

In Fig. 4 we observe a positive flat peak [0.19 (3) e Å^{-3}] in the midpoint of the Co—Co bond [2.4402 (2) Å] and the peaks closer to the Co atoms are indicative of the metal–ligand interactions. In the model deformation density maps of the orthorhombic form of (3) [Bianchi *et al.*, 2001; Co—Co 2.4222 (3) Å] and of $Co_2(CO)_6(AsPh_3)_2$ [Macchi *et al.*, 1998; Co—Co 2.6430 (2) Å] the flat peaks in the midpoint of the metal–metal bond are 0.43 (6) and 0.00 (5) e Å^{-3}, respectively. The differences of electron density accumulation in the middle of the metal–metal bond for the above complexes might be attributed to different metal–metal distances and possibly to different multipole models used to fit the X-ray data.

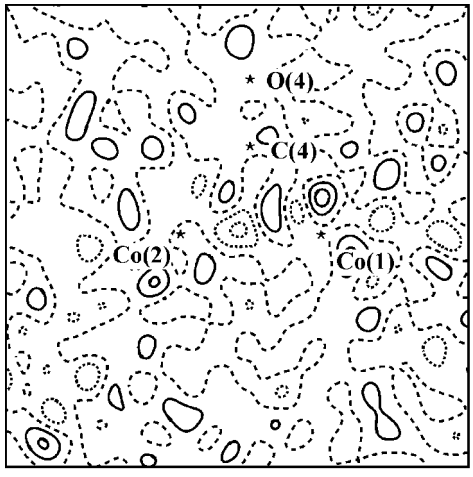

(*a*)

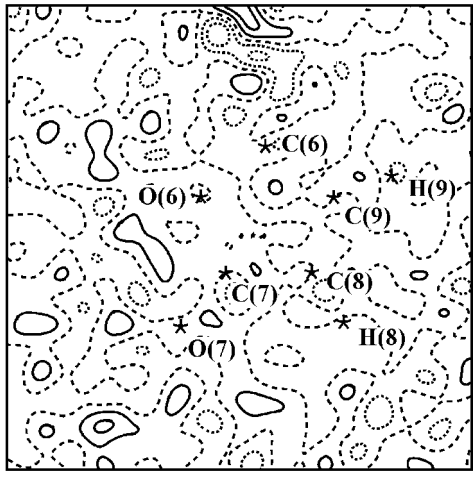

(*b*)

Figure 3
Residual density in (*a*) the Co(1)—Co(2)—C(4) plane and (*b*) in the γ-lactonic plane. The contour interval is 0.10 e Å^{-3}. Solid lines positive, short dashed lines negative, wide dashed line zero contour.

Table 4
Net atomic charges (e) from the multipole refinement.

Atom	Charge (e.s.d.)
Co(1)	0.3 (1)
Co(2)	0.3 (1)
C(1′)	0.0 (1)
O(1′)	−0.13 (8)
C(2′)	0.1 (1)
O(2′)	0.04 (9)
C(3′)	0.2 (1)
O(3′)	0.17 (9)
C(4)	0.10 (9)
O(4)	−0.06 (7)
C(5′)	0.1 (1)
O(5′)	−0.02 (8)
C(6′)	−0.1 (1)
O(6′)	0.16 (9)
C(7′)	−0.1 (1)
O(7′)	0.0 (1)
C(6)	−0.18 (7)
C(7)	−0.33 (9)
C(8)	−0.2 (1)
C(9)	−0.28 (8)
O(6)	−0.02 (5)
O(7)	−0.12 (7)
H(8)	0.05 (9)
H(9)	0.02 (7)

3.4. Topological properties

The results of the topological analysis of the experimental ED for the title compound are reported in Tables 5 and 6 for intramolecular bonds and intermolecular contacts, respectively.

Fig. 5 reports the Laplacian maps in the Co(1)Co(2)C(4) and γ-lactonic planes of $Co_2(CO)_6(\mu\text{-}CO)(\mu\text{-}C_4O_2H_2)$, showing a more detailed description of atomic interactions.

The Laplacian map (Fig. 5*a*) between and around the two Co atoms shows a wide zone of positive values and a contraction of the electron density toward the nuclei. The trend of Laplacian distribution in the γ-lactonic ring (Fig. 5*b*) is typical of covalent 'shared' interactions for the C—C and the C—H bonds, while for the C—O bonds it exhibits a partial polar character. The very weak hydrogen-bond interaction, C(8)—H(8)···O(1′), displays the peculiar topological characteristics of the closed-shell interactions, with a positive and small value of the Laplacian in the bonding region.

The number of BCP's found in the experimental ED corresponds to the expected number of bonds for (3), including the interaction between the two Co atoms. A (3,−1) bond critical point with a small ρ_b [0.46 (2) e Å^{-3}] was found for the Co—Co bond [2.4402 (2) Å] of (3). The ρ_b and bond distance (R_e) values found in other compounds are: in $Mn_2(CO)_{10}$ ρ_b = 0.190 (4) e Å^{-3} and Mn—Mn = 2.9042 (8) Å (Bianchi *et al.*, 2000), in $Co_2(CO)_6(AsH_3)_2$ ρ_b = 0.204 (11) e Å^{-3} and Co—Co = 2.6430 (2) Å (Macchi *et al.*,

1998), in $Co_4(CO)_{11}(PPh_3)$ $\rho_b = 0.252$ (3) e Å^{-3} and Co—Co = 2.528 (8) Å (Macchi *et al.*, 1999), and in the orthorhombic phase of $Co_2(CO)_6(\mu\text{-CO})(\mu\text{-}C_4O_2H_2)$ $\rho_b = 0.76$ (6) e Å^{-3} and Co—Co = 2.4222 (3) Å (Bianchi *et al.*, 2001). The above values show a reverse trend of ρ_b with respect to the bond distance R_e. The small absolute values of the λ_1 and λ_2 curvatures at the BCP of the metal–metal bond are in agreement with a flat $\rho(\mathbf{r})$ in the interatomic surface (Silvi & Gatti, 2000). The (3,+1) ring critical points associated to the two Co_2C rings are located fairly close (0.24 Å average) to the Co—Co BCP. This is a clear indication of a molecular structure very close to an unstable configuration which would occur when the two ring critical points coalesce with the Co—Co BCP (Bader, 1990). The Co—Co bond path is almost linear and it is displaced 0.13 Å from the internuclear axis in the direction opposite to that claimed by the bent Co—Co bond model (Low *et al.*, 1991).

In the experimental ED study of $Co_4(CO)_{11}(PPh_3)$ (Macchi *et al.*, 1999) no BCP's with the corresponding bond path were found for the three carbonyl-bridged Co—Co bonds and the authors assert that the Co—C—Co bond is a delocalized three-center interaction and that the metal–metal bonding is indirect because it is achieved through the carbonyl. At this point, the two different experimental analyses suggest that the Co—Co interaction with bridged ligands is close to the borderline between bonding and non-bonding interactions.

A positive $\nabla^2\rho_b$ (in the range 0.8–8.6 e Å^{-5}) and a low value of ρ_b (in the range 0.46–1.24 e Å^{-3}) classify as 'closed-shell' the Co—Co and Co—C bonds. The G_b and $|V_b|$ values for these bonds are comparable and the resulting energy densities

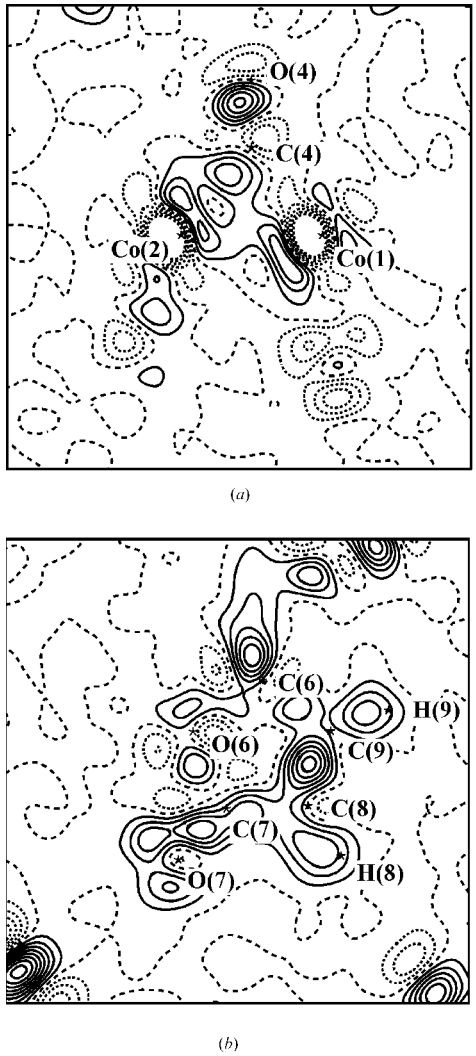

Figure 4
Dynamic model deformation densities (*a*) in the Co(1)—Co(2)—C(4) plane and (*b*) in the γ-lactonic plane. The contour interval is 0.10 e Å^{-3}. Solid lines positive, short dashed lines negative, wide dashed line zero contour.

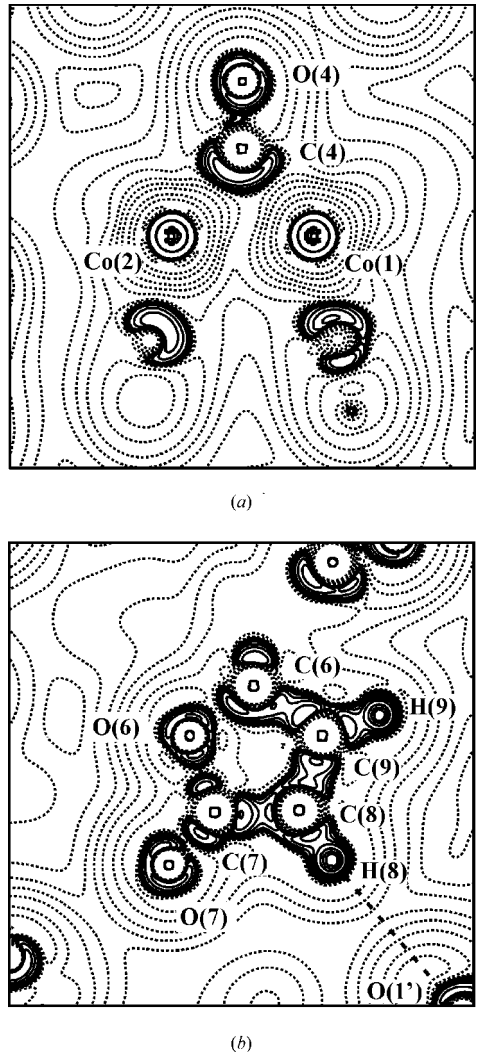

Figure 5
Laplacian, $\nabla^2\rho(\mathbf{r})$, of the experimental electron density map in (*a*) the Co(1)—Co(2)—C(4) plane and (*b*) in the γ-lactonic plane. The values of the contours (a.u.) increase from the outermost one inwards in steps of 2×10^n, 4×10^n, 8×10^n with n beginning at -3 and increasing in steps of 1. Positive values are denoted by dashed contours, negative are denoted by solid contours.

Table 5
Bond critical point properties.

R_e = distance between atoms X and Y; R_b = bond path length.

$X-Y$	R_e (Å)	R_b (Å)	ρ_b (e Å^{-3})	$\nabla^2\rho_b$ (e Å^{-5})	λ_1 (e Å^{-5})	λ_2 (e Å^{-5})	λ_3 (e Å^{-5})
Intramolecular interactions							
Co(1)—Co(2)	2.4402 (2)	2.5626	0.46 (2)	3.4 (3)	−2.0	−1.0	6.4
Co(1)—C(1′)	1.809 (2)	1.860	1.24 (5)	3.5 (6)	−9.3	−6.9	19.7
Co(1)—C(2′)	1.829 (2)	1.861	1.06 (5)	2.9 (5)	−8.3	−6.2	17.4
Co(1)—C(3′)	1.856 (2)	1.896	0.85 (4)	3.3 (7)	−6.0	−4.9	14.2
Co(1)—C(4)	1.943 (2)	2.107	0.61 (3)	4.8 (3)	−3.6	−2.6	11.0
Co(1)—C(6)	1.989 (2)	2.046	0.86 (4)	0.8 (3)	−6.1	−4.5	11.4
Co(2)—C(4)	1.929 (2)	1.975	0.75 (4)	8.6 (4)	−4.0	−2.4	15.0
Co(2)—C(5′)	1.811 (2)	2.107	0.52 (4)	2.7 (3)	−3.7	−2.9	9.3
Co(2)—C(6)	1.990 (2)	2.020	1.11 (3)	1.6 (2)	−7.8	−5.6	15.0
Co(2)—C(6′)	1.825 (2)	1.856	1.13 (5)	6.9 (6)	−8.6	−4.7	20.2
Co(2)—C(7′)	1.852 (2)	1.856	1.01 (5)	4.3 (9)	−7.2	−6.5	18.0
C(1′)—O(1′)	1.139 (3)	1.143	3.6 (2)	−10 (4)	−49	−33	72
C(2′)—O(2′)	1.135 (4)	1.147	3.2 (2)	−4 (3)	−41	−33	70
C(3′)—O(3′)	1.131 (4)	1.165	3.4 (2)	−36 (6)	−40	−35	39
C(4)—O(4)	1.163 (3)	1.178	2.5 (2)	−15 (6)	−29	−17	31
C(5′)—O(5′)	1.137 (4)	1.138	3.4 (2)	−30 (5)	−40	−34	44
C(6′)—O(6′)	1.134 (3)	1.134	3.6 (2)	−29 (3)	−49	−30	50
C(7′)—O(7′)	1.133 (4)	1.132	3.4 (3)	−23 (8)	−42	−32	51
C(6)—O(6)	1.406 (3)	1.425	1.87 (9)	−8 (3)	−15	−14	21
C(6)—C(9)	1.465 (3)	1.493	1.65 (7)	−12 (2)	−12	−10	10
O(6)—C(7)	1.382 (3)	1.386	2.1 (1)	−17 (2)	−21	−13	17
C(7)—O(7)	1.207 (4)	1.241	3.2 (1)	−25 (13)	−30	−26	31
C(7)—C(8)	1.462 (4)	1.466	1.77 (8)	−9 (1)	−12	−9	12
C(8)—C(9)	1.346 (3)	1.360	2.3 (1)	−22 (5)	−19	−14	11
C(8)—H(8)	1.03 (3)	1.03	2.0 (1)	−15 (4)	−19	−16	20
C(9)—H(9)	1.05 (3)	1.06	1.81 (8)	−15 (2)	−18	−17	20
Intramolecular ring points							
Co(1)—Co(2)—C(4)			0.44 (2)	4.0 (1)	−1.8	1.5	4.3
Co(1)—Co(2)—C(6)			0.45 (3)	5.7 (3)	−2.5	1.2	7.0
C(6)—O(6)—C(7)—C(8)—C(9)			0.40 (2)	5.8 (2)	−1.2	2.6	4.4

E_b^e have negative values (magnitudes below 1.1 hartree Å^{-3}). Similar values of the mentioned topological parameters were found in the experimental ED analysis of $Co_2(CO)_6(AsPh_3)_2$ (Macchi *et al.*, 1998). In the conclusions of this paper the authors consider, however, the Co—Co bond as a 'genuine covalent bond', having a 'shared' character on the basis of G_b/ρ_b and E_b^e parameters. They suggest to emphasize less the values of ρ_b and $\nabla^2\rho_b$ (Fig. 6 and Table 4 in Macchi *et al.*, 1998) that, on the other hand, seem to clearly indicate a 'closed-shell' character for the Co—Co bond. Previous topological analyses of the experimental ED on a number of organometallic and coordination compounds (Bianchi *et al.*, 1998, 2000, 2001, and references therein) suggested that metal–metal bonds and metal–ligand bonds have topological properties intermediate between covalent and ionic bonds.

In a molecule of (3) there are three chemically different C—O bonds: the terminal and bridging carbonyl C⋮⋮O bonds, and the C═O and C—O bonds along the γ-lactonic ring. The C—O distances characterize the terminal [1.135 (4) Å av.] CO's, the bridging C(4)═O(4) [1.163 (3) Å], the formally double C(7)═O(7) bond [1.207 (4) Å] and the formally single C(6)—O(6) bond [1.394 (3) Å average]; to shorter bond distances roughly correspond greater values of ρ_b. While the ρ_b and $\nabla^2\rho_b$ values do not differ significantly in the terminal and bridging CO's, the map of Laplacian (Fig. 5*a*) shows for μ-CO an enlargement of the VSCC region directed toward the two Co atoms, compared with the VSCC of each terminal CO which points toward just one Co atom. The formally double bond C(7)═O(7) and the C⋮⋮O bonds of carbonyl ligands are characterized (Table 5) by quite similar (within the errors) high values of ρ_b (3.4 e Å^{-3} average) and large negative values of $\nabla^2\rho_b$ (−25 e Å^{-5} average). The formally C(6)—O(6) and C(7)—O(6) single bonds have on average smaller values of ρ_b and smaller negative values of $\nabla^2\rho_b$. As expected, the topological values of all CO bonds are in agreement with those of typical covalent bonds.

3.5. Intermolecular interactions

In Table 6 are listed the intermolecular interactions, for which a bond path was found. The ρ_b and $\nabla^2\rho_b$ of these interactions are in the range 0.02–0.05 e Å^{-3} and 0.31–0.66 e Å^{-5}, respectively. With the exception of very weak hydrogen bonds [C(9)···O(3′) 3.78 Å, C(9)—H(9)···O(3′) 148°; C(8)···O(1′) 3.73 Å, C(8)—H(8)···O(1′) 169°; Desiraju, 1991], the predominant intermolecular interactions are O···O contacts (see Table 3) and they have no preferential directions. On the contrary, in the orthorhombic form of (3) (Bianchi *et al.*, 2001) the C—H···O hydrogen bonds are more important and roughly lay on planes parallel to the (100) face; in fact, the orthorhombic crystals of (3) are easily split into laminae along this face.

The flat distribution of $\rho(\mathbf{r})$ in the intermetallic zone allows for easy variations of the Co—Co bond length, which may be therefore induced by the changes in the packing arrangement. In fact, the Co—Co distance [2.4402 (2) Å in the triclinic form at 120 K and 2.4222 (3) Å in the orthorhombic form at 150 K] is the most relevant geometrical difference between the molecules in the two phases. The BCP properties of the weak interactions, reported in Table 6, even if slightly significant from a statistical point of view, are at the limit of experimental accuracy. However, they are very close to those observed for $Mn_2(CO)_{10}$ and for the orthorhombic polymorph of (3); therefore, it appears that the multipole model reproduces well the effects of intermolecular interactions.

4. Conclusions

The present experimental ED study of the triclinic form of $Co_2(CO)_6(\mu\text{-}CO)(\mu\text{-}C_4O_2H_2)$ confirms the presence of a

Table 6
Bond critical point properties for the intermolecular contacts.

$X\cdots Y$	ρ_b (e Å^{-3})	$\nabla^2\rho_b$ (e Å^{-5})	λ_1 (e Å^{-5})	λ_2 (e Å^{-5})	λ_3 (e Å^{-5})	G_b (hartree Å^{-3})	G_b/ρ_b (hartree e^{-1})	V_b (hartree Å^{-3})	E_b^e (hartree Å^{-3})
O(7)···C(5′)^{ii}	0.05 (1)	0.62 (5)	−0.10	−0.06	0.79	0.03	0.69	−0.02	0.01
C(8)···O(5′)^{iii}	0.04 (1)	0.59 (5)	−0.11	−0.03	0.73	0.03	0.78	−0.02	0.01
C(8)···O(7′)^{ii}	0.03 (1)	0.43 (5)	−0.07	−0.01	0.51	0.02	0.75	−0.01	0.01
H(8)···O(1′)^{iv}	0.03 (1)	0.48 (5)	−0.09	−0.09	0.66	0.03	0.82	−0.02	0.01
H(9)···O(3′)^{v}	0.02 (1)	0.40 (5)	−0.07	−0.07	0.54	0.02	0.99	−0.01	0.01
O(4)···O(4)^{vi}	0.04 (1)	0.66 (5)	−0.11	−0.03	0.80	0.03	0.86	−0.02	0.01
O(4)···O(2′)^{vi}	0.03 (1)	0.49 (5)	−0.08	−0.04	0.61	0.02	0.84	−0.02	0.00
O(4)···O(3′)^{v}	0.03 (1)	0.44 (5)	−0.07	−0.05	0.56	0.02	0.76	−0.01	0.01
O(4)···O(7′)^{v}	0.02 (1)	0.35 (5)	−0.05	−0.04	0.44	0.02	0.88	−0.01	0.01
O(4)···O(6′)^{vi}	0.04 (1)	0.61 (5)	−0.11	−0.06	0.78	0.03	0.81	−0.02	0.01
O(1′)···O(3′)^{v}	0.03 (1)	0.48 (5)	−0.09	−0.05	0.62	0.02	0.82	−0.02	0.00
O(1′)···O(5′)^{vii}	0.03 (1)	0.42 (5)	−0.07	−0.03	0.52	0.02	0.73	−0.01	0.01
O(1′)···O(6′)^{vii}	0.03 (1)	0.45 (5)	−0.06	−0.04	0.55	0.02	0.78	−0.01	0.01
O(2′)···O(7′)^{ix}	0.04 (1)	0.58 (5)	−0.10	−0.06	0.74	0.03	0.77	−0.02	0.01
O(2′)···O(6′)^{ix}	0.03 (1)	0.45 (5)	−0.07	−0.04	0.56	0.02	0.78	−0.01	0.01
O(5′)···O(5′)^{iii}	0.02 (1)	0.36 (5)	−0.05	−0.04	0.45	0.02	0.90	−0.01	0.01
O(5′)···O(7′)^{ii}	0.04 (1)	0.62 (5)	−0.10	−0.09	0.82	0.03	0.82	−0.02	0.01
O(5′)···O(7′)^{v}	0.04 (1)	0.60 (5)	−0.10	−0.08	0.78	0.03	0.79	−0.02	0.01
O(3′)···O(6′)^{ix}	0.02 (1)	0.31 (5)	−0.05	−0.02	0.38	0.02	0.78	−0.01	0.01

For symmetry codes see footnote to Table 3.

cobalt–cobalt bond in a system with bridging ligands in a folded Co_2C_2 moiety, as already found in the topological analysis of its orthorhombic form (Bianchi *et al.*, 2001). The flat electron density around the Co—Co BCP and around the Co_2C ring critical points is a peculiar feature of the metal–metal bond in the title compound.

The values of ρ_b, $\nabla^2\rho_b$, G_b, V_b and E_b^e parameters observed for the 'closed-shell' Co—Co, Co—C_{CO} bonds and intermolecular interactions agree with the bonding classification given in a previous paper (Bianchi *et al.*, 2000).

This analysis confirms the ability of the multipole model to reproduce the weak O···O, O···C and O···H interactions, and also when heavy atoms are present in the crystal structure.

We thank MURST (*Cofin*98) for financial support.

References

Abramov, Yu. A. (1997). *Acta Cryst.* A**53**, 264–272.
Bader, R. F. W. (1990). *Atoms in Molecules – A Quantum Theory.* Oxford University Press.
Barzaghi, M. (2001). *PAMoC (Version 2001.0), Online User's Manual.* Centro del CNR per lo Studio delle Relazioni tra Struttura e Reattività Chim, Milano, Italy, 2001 (www.csrsrc.mi.cnr.it/~barz/pamoc/).
Bianchi, R., Gervasio, G. & Marabello, D. (1998). *Chem. Commun.* pp. 1535–1536.
Bianchi, R., Gervasio, G. & Marabello, D. (2000). *Inorg. Chem.* **39**, 2360–2366.
Bianchi, R., Gervasio, G. & Marabello, D. (2001). *Helv. Chim. Acta*, **84**, 722–734.
Blessing, R. H. (1987). *Cryst. Rev.* **1**, 3–58.
Blessing, R. H. (1989). *J. Appl. Cryst.* **22**, 396–397.
Braterman, G. (1972). *Struct. Bonding (Berlin)*, **10**, 57–65.
Clementi, E. & Roetti, C. (1974). *At. Data Nucl. Data Tables*, **14**, 177–478.
Cruickshank, D. W. J. (1949). *Acta Cryst.* **2**, 65–82.
Desiraju, G. R. (1991). *Acc. Chem. Res.* **24**, 290–296.
De Titta, G. T. (1985). *J. Appl. Cryst.* **18**, 75–79.
Espinosa, E., Molins, E. & Lecomte C. (1998). *Chem. Phys. Lett*, **285**, 170–173.
Gardner Sumner, G., Klug, H. P. & Alexander, L. E. (1964). *Acta Cryst.* **17**, 732–742.
Greenfield, H., Sternberg, H. W., Friedel, R. A., Wotiz, J., Markby, R. & Wender, J. (1956). *J. Am. Chem. Soc.* **77**, 3951.
Hansen, N. K. & Coppens, P. (1978). *Acta Cryst.* A**34**, 909–921.
Hehre, W. J., Ditchfield, R., Stewart, R. F. & Pople, J. A. (1970). *J. Chem. Phys.* **52**, 2769–2773.
Heijser, W., Baerends, E. J. & Ross, P. (1980). *Discuss. Faraday Soc. (Symp.)* **14**, 211–234.
Hirshfeld, F. (1976). *Acta Cryst.* A**32**, 239–244.
Johnson, C. K. (1965). *ORTEP*. Report ORNL-3794. Oak Ridge National Laboratory, Tennessee, USA.
Leung, P. C. & Coppens, P. (1983). *Acta Cryst.* B**39**, 535–541.
Low, A. A. & Hall, M. B. (1993). *Inorg. Chem.* **32**, 3880–3889.
Low, A. A., Kunze, K. L. & MacDougall, P. J. (1991). *Inorg. Chem.* **30**, 1079–1086.
Macchi, P., Garlaschelli, L., Martinengo, S. & Sironi, A. (1999). *J. Am. Chem. Soc.* **121**, 10428–10429.
Macchi, P., Proserpio, D. M. & Sironi, A. (1998). *J. Am. Chem. Soc.* **120**, 13429–13435.
Mills, O. S. & Robinson, G. (1967). *Inorg. Chim. Acta*, **1**, 61–63.
Pályi, G., Váradi, G. & Markó, L. (1986). *Stereochemistry of Organometallic and Inorganic Compounds*, edited by I. Bernal, Vol. 1, pp. 358–373. Amsterdam, Oxford, New York, Tokyo: Elsevier Science.
Siemens (1996). Siemens Energy and Autom. Inc., Madison, Wisconsin, USA.
Silvi, B. & Gatti C. (2000). *J. Phys. Chem. A*, **104**, 947–953.
Sternberg, H. W., Shukys, J. G., Delle Donne, C., Markby, R., Friedel, R. A. & Wender, I. (1959). *J. Am. Chem. Soc.* **81**, 2339–2342.
Stewart, R. F. & Spackman, M. A. (1983). *VALRAY User's Manual.* Department of Chemistry, Carnegie-Mellon University, Pittsburg.